Supplementary Information (SI) for Journal of Materials Chemistry B.

SUPPORTING INFORMATION

Hydrothermally transformed multifunctional proteinaceous nanoparticle biosealant with intrinsic light-responsive redox cycling for self-sterilizing and accelerated wound healing

Maansi Aggarwal[a] , Purnendu Ghosh[b], K.P. Mohithraj[b], Samiran Mondal[c], Dinesh Kumar Kotnees[d], Samit Kumar Nandi[b*] , Prolay Das[a*]

[a] Department of Chemistry, Indian Institute of Technology Patna, Patna 801103, Bihar, India

[b] Department of Veterinary Surgery and Radiology, West Bengal University of Animal and Fishery Science, Belgachia, Kolkata 700037, India

[c] Department of Veterinary Pathology, West Bengal University of Animal and Fishery Science, Belgachia, Kolkata 700037, India

[d] Department of Metallurgical and Materials Engineering, Indian Institute of Technology Patna, Patna 801103, Bihar, India

Corresponding authors: prolay@iitp.ac.in, samitnandi1967@gmail.com

Materials

Reagent-grade acrylamide, tannic acid, nitroblue tetrazolium, riboflavin, methionine, salicylic acid, and DPX were purchased from Sisco Research Laboratories Pvt. Ltd., India, and used without purification. Gelatin, Mayor's hematoxylin, eosin, 2% w/v, paraffin (melting point 58-60°C), Mueller-Hinton Agar (MHA), Agar-agar powder, nutrient broth, penicillin-G, and streptomycin sulphate were purchased from Himedia, India. ABTS, Dihydrorhodamine123, benzoylated dialysis membrane with a cutoff MWCO of 2 kDa, xylene, HCl, H_2O_2, Tween 20, and NMR grade D_2O were procured from Merck, India. Primary and secondary antibodies were procured from Invitrogen (Anti-Rabbit monoclonal pAb) and VECTASTAIN® ABC-HRP Kit and Peroxidase. For surgical procedures, xylazine hydrochloride, ketamine hydrochloride, povidone-iodine (Betadine), and thiopentone sodium (Thiosol) from Indian Immunologicals Ltd, Themis Medicare, Win-Medicare Pvt. Ltd., and Neon Laboratories Ltd. were acquired. Bacterial strains *Escherichia coli* (MTCC 443), *Staphylococcus aureus* (MTCC 96), *Bacillus subtilis* (MTCC 441), and *Kebsiella pneumoniae* (MTCC 618) with respective serial numbers were used.

Instrumentation

The conformational changes in gelatin proteinaceous nanoparticle (PNP) were determined by powder X-ray diffraction (XRD) of purified PPD, and PPD sealant using a Rigaku TTRX-III diffractometer equipped with a Cu Kα radiation source (λ = 1.54 Å). Field emission scanning electron microscopy (FESEM) imaging was carried out on Au-coated lyophilized samples using a Gemini SEM500 microscope (ZEISS). Hydrodynamic radii of samples were measured via dynamic light scattering (DLS) using Beckman Coulter's Delsa instrument, while zeta potential values were obtained from a Litesizer 500 analyzer (Anton Paar).

For functional determination, Fourier transform infrared (FTIR) spectra were collected on a PerkinElmer Spectrum 400 spectrometer from KBr pellets over the range 4000 – 400 cm^{-1}. ^1H NMR (JEOL 500 MHz) in D_2O-d_2 confirmed the grafting of TA groups on PNP. ^{13}C CPMAS NMR analyses on JEOL 500 MHz of PNP and PNP sealant were conducted to verify TA post-grafting.

Detailed optical studies were acquired by UV–vis absorption spectra on a UV-2550 spectrophotometer (Shimadzu, Japan). Steady-state fluorescence spectra of PNPs and their conjugates were recorded using a Horiba Jobin Yvon Fluoromax-4P spectrofluorometer. Circular dichroism (CD) spectra were collected using a JASCO 150 spectropolarimeter over the 185–300 nm range at a scan rate of 100 nm/min in a 1 cm path length cuvette. A reverse phase high performance liquid chromatography (RP-HPLC) system (controller: CBM-20Alite, pump: LC-20AD, PDA detector: SPD-M20A; Shimadzu, Kyoto, Japan) with an enable C18G column (250 × 4.6 mm) was used for obtaining HPLC chromatograms using acetonitrile/sodium phosphate buffer to check stability of PNP sealant over four months.

Thermal gravimetric analysis (TGA) was performed using a TA Instruments Q600 SDT at 10 °C/min under N_2 from 28-1000°C. Lap shear studies with PNP and PNP sealant on porcine skin models were conducted using a Zwick-Roell Z010 universal testing machine (Germany). The treated porcine skin was cut into rectangular halves (30 mm x 15 mm), pressed against matching skin pieces for 30 min. Adhesive was evenly applied to the dermis side of one piece and fully covered with another, creating a 15 × 15 mm overlap and pressed against matching skin pieces for 30 min, followed by curing at 37°C and 50% humidity for 2 h. All the histological and immunohistology images were captured using a light and fluorescence microscope (Leica DM 2000, Germany).

Characterization of physico-mechanical properties of PNP sealant

At room temperature, all rheological measurements were performed using a commercial stress-controlled rheometer (MCR-302, Anton Paar, Austria). A flat cylindrical steel probe, operating at a fixed rate of 0.1 mm/s, was employed to record force–displacement profiles during bonding and debonding phases. Oscillatory sweep tests were conducted in parallel-plate geometry (8 mm diameter, 1 mm gap) to monitor the storage modulus (G′) and loss modulus (G″) in real time. Using a constant shear strain of 0.01%, selected from the linear viscoelastic region in the strain sweep, frequency sweep measurements were performed across a range of 0.01–625 Hz, from low to high oscillation frequencies.

Porcine skin preparation for tensile strength test

Fresh porcine skin from a local slaughterhouse was prepared for the lap shear test. Dorsal sections (30 × 15 mm) were washed with warm water, the subcutaneous fat was removed with a scalpel, and the dermal layer was cleaned using gauze and isopropyl alcohol (ASTM F2255-2015). The tissue was soaked in 0.9% saline to retain moisture, then coated with nanoglue over a 15 × 15 mm overlap and dried at room temperature for 30 min.

RP-HPLC Study

A mobile phase comprising 10 mM sodium phosphate buffer (pH 7.4) and acetonitrile (60:40, v/v) was employed for RP-HPLC analysis of PNP sealant from different batches at a flow rate of 0.2 mL/min. PNP sealant samples (5 µL) were injected, and chromatograms were recorded at a detection wavelength of 278 nm.

Histological section and H&E staining

Formalin-fixed tissues were processed for routine hematoxylin and eosin (H&E) staining. Samples were embedded in paraffin wax (60 °C), trimmed, and sectioned at 5 µm using a rotary microtome. Paraffin ribbons were floated on a 45 °C water bath, mounted on positively charged slides, and air-dried. Slides were deparaffinized in fresh xylene (2 × 5 min), rehydrated through descending ethanol series (100%, 90%, 70%, 50%; 2–3 min each), and rinsed in distilled water.

Nuclei were stained with Mayer's hematoxylin (8 min), rinsed (5 min tap water), differentiated in acid alcohol (1% HCl in 70% ethanol), and washed again. Cytoplasm and extracellular matrix were counterstained with eosin (1–2 min) and rinsed. Dehydration was performed through ascending ethanol series (50%, 70%, 90%, and 100%) followed by xylene clearing (2 × 5 min). Finally, slides were mounted with DPX, coverslipped, and examined under a light microscope for histopathological evaluation.

Masson's trichrome staining

Masson's Trichrome staining was performed on 5 μm formalin-fixed, paraffin-embedded sections following standard protocols with minor modifications.[1] Sections were deparaffinized in xylene, rehydrated using graduated ethanol to distilled water, and then treated with Bouin's solution at 60 °C for 1 h. Nuclei were stained with Weigert's iron hematoxylin (10 min), cytoplasm with Biebrich scarlet–acid fuchsin (10 –15 min), and collagen differentiated using phosphomolybdic–phosphotungstic acid (10 min) before counterstaining with aniline blue (5 – 10 min). Slides were rinsed in 1% acetic acid (2 min), dehydrated, cleared in xylene, and mounted using DPX and examined microscopically.

Reticulin staining

Formalin-fixed tissue slices with paraffin-embedded (5 μm) were deparaffinized in xylene and then rehydrated using distilled water and graded ethanol. After 5 min of oxidation in 1% potassium permanganate, the sections were bleached in 2% oxalic acid. Slides were rinsed, sensitized for 10 min in 10% iron alum, and then impregnated for 30 min with an ammoniacal silver solution. Sections were toned in auric chloride, fixed in sodium thiosulfate, and reduced in formalin. Slides were thoroughly cleaned, dehydrated, cleared, and then counterstained with nuclear fast red before being mounted using DPX. Under light microscopy, reticular fibers were black.

CD31 immunohistochemistry (IHC) assay

IHC test was performed on 5 μm formalin-fixed paraffin-embedded (FFPE) sections mounted on coated glass slides. Ribbon-containing tissue slices were then placed in water, and the best tissue sections were picked out, together with the surrounding paraffin mass, and placed on the charged glass slides. After that, the slides were allowed to air dry at room temperature. Sections were deparaffinized in xylene, rehydrated through graded ethanol (100–50%), and rinsed in distilled water. Antigen retrieval was carried out in citrate buffer (pH 6.0) at 96 °C for 30 min, followed by endogenous peroxidase blocking with 3% H_2O_2 for 30 min. After PBS-Tween 20 (PBST) washes, slides were blocked with serum for 30 min at 37 °C. Subsequently incubated overnight at 4°C with anti-rabbit CD31 (PECAM-1, Invitrogen), and then washed with PBST. HRP-conjugated secondary antibody was applied for 30 min at room temperature, followed by incubation with ABC reagent (VECTASTAIN® ABC-HRP Kit) for 30 min at 37°C. Afterward, they were incubated with DAB substrate for 15 minutes at room temperature to develop the colour. After applying a haematoxylin counterstain, the slides were once more cleaned with distilled water. Slides were then mounted in DPX with cover slips following a dehydration process that involved dipping them into progressively stronger alcohol and finishing with a xylene wash.

Analysis of collected regenerative tissue from wound site: histological, extracellular matrix deposition and immunohistochemical evaluation

Histological analysis was performed on skin wound sections collected on days 2 and 7 post-treatment. Wound tissues were fixed in 10% neutral buffered formalin and sectioned at 5 µm thickness using a cryomicrotome. Sections were stained with H&E, Masson's trichrome, reticulin, and CD31 to assess tissue regeneration, inflammation, extracellular matrix remodeling, and angiogenesis. H&E staining was used to evaluate epithelial regeneration and inflammatory cell infiltration. Collagen deposition and organization were examined using Masson's trichrome staining, while reticulin staining was used to visualize reticular fiber formation. CD31 immunostaining was performed to assess endothelial cell activity and neovascularization.

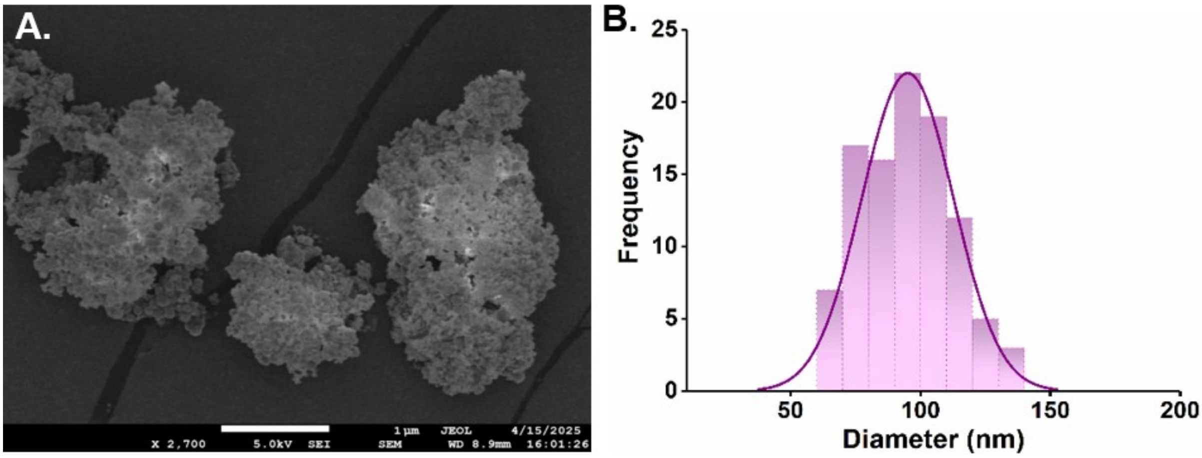

Fig. S1. A. FESEM image of PNP with an average size of 100 nm, and B. Average size distribution of PNP calculated using ImageJ.

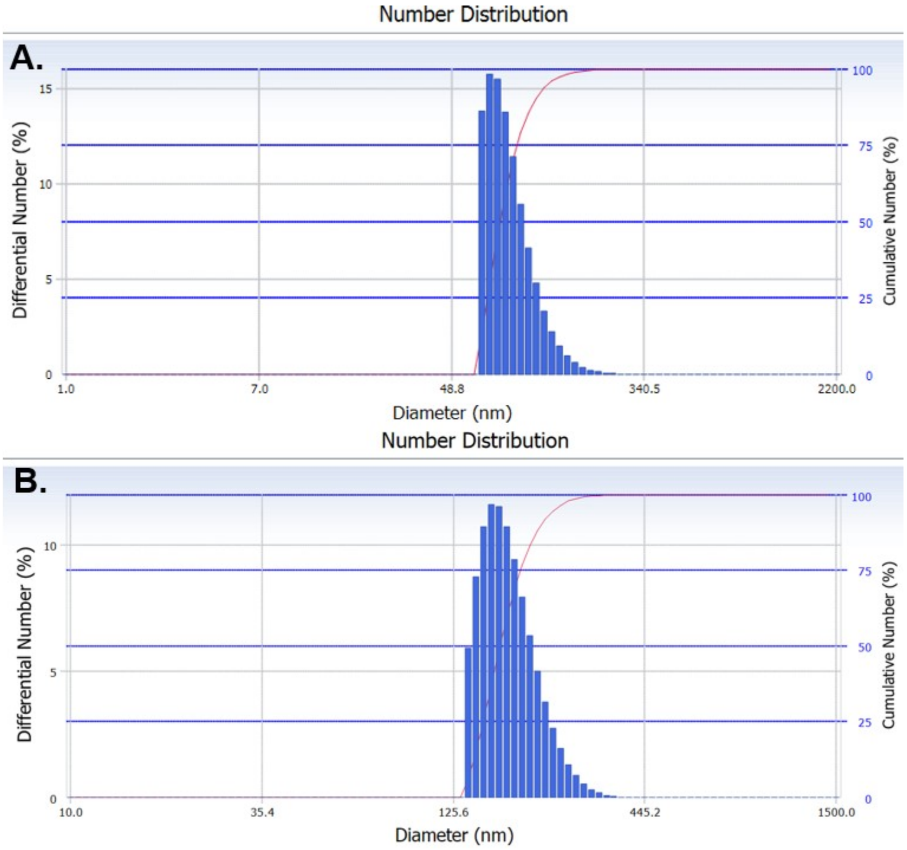

Fig. S2. DLS spectra with the hydrodynamic diameter of A. PNP as 154 nm and B. PNP sealant as 227 nm.

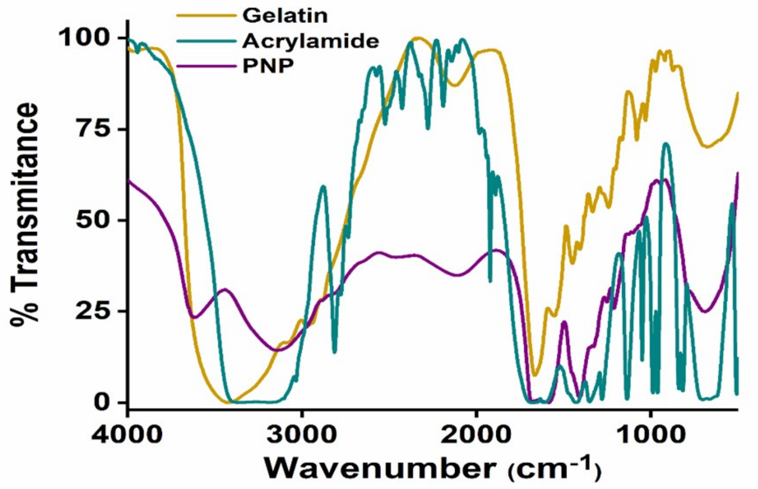

Fig. S3. FTIR spectra confirm that PNP is upholding integral functionalities of gelatin while showing changes in amide-A peaks and no corresponding peaks of acrylamide.

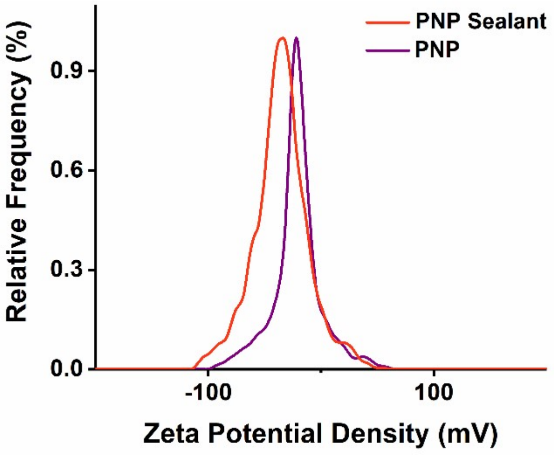

Fig. S4. Zeta potential spectra showing negative surface shifted from -12.3 mV in PNP to -31.5 mV in PNP sealant arising from the ionisation of the polyphenolic group.

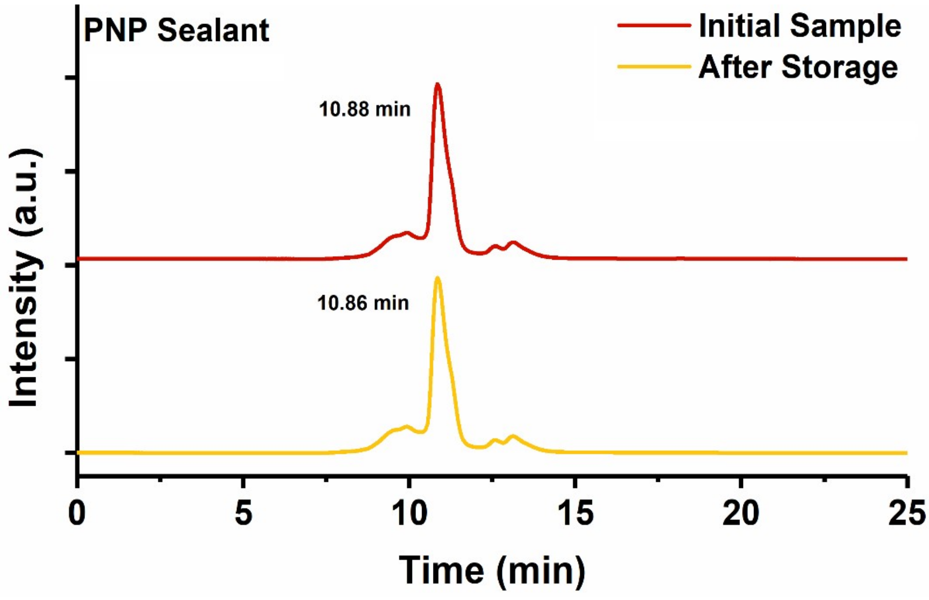

Fig. S5. RP-HPLC chromatogram demonstrating similar retention time over the four months of storage, indicating high shelf life.

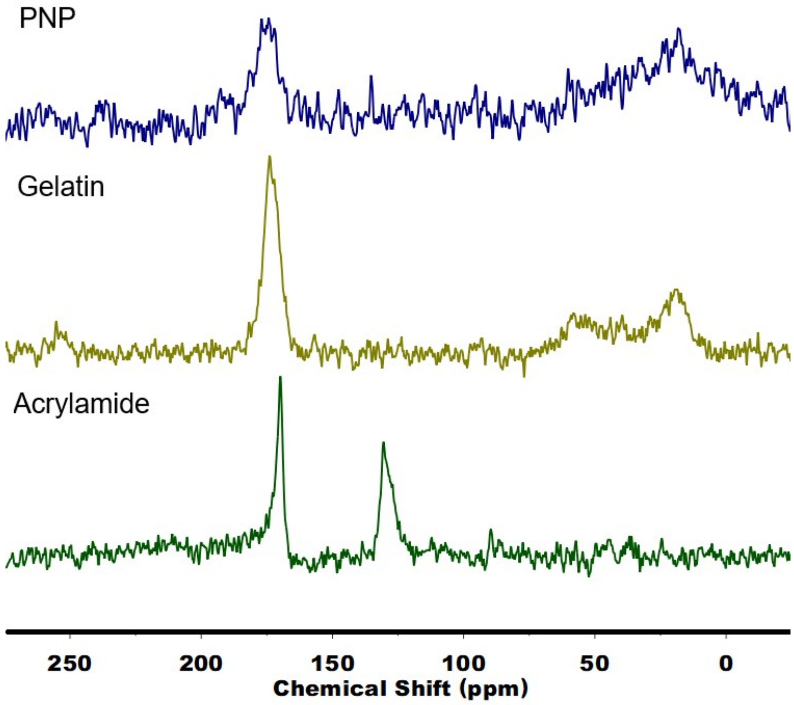

Fig. S6. ^{13}C CPMS spectra of PNP have similar peaks to gelatin while the double bond of acrylamide is covalently conjugated.

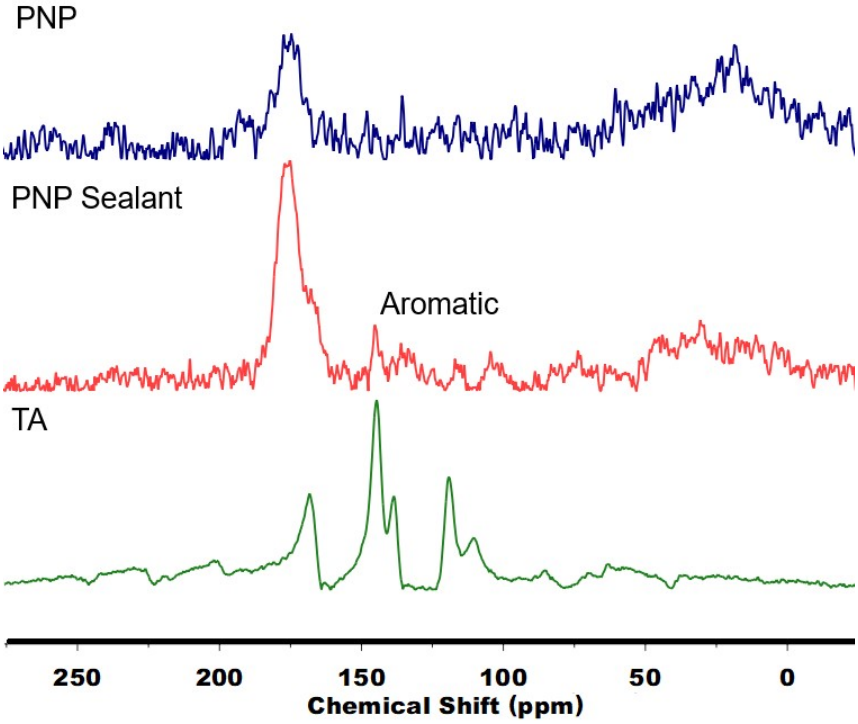

Fig. S7. ^{13}C CPMS confirms post-modification of PNP with TA with aromatic peaks.

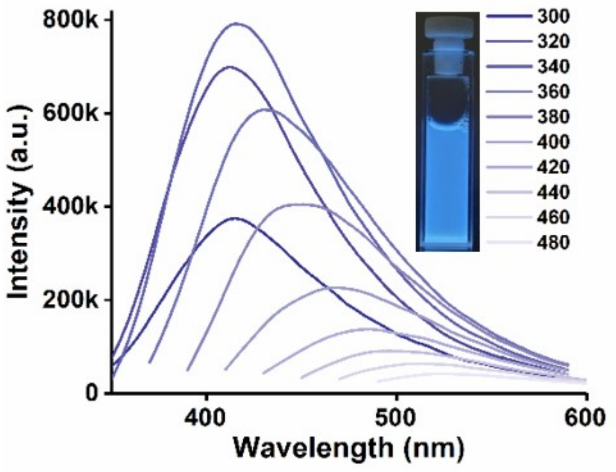

Fig. S8. Excitation-dependent steady-spectra of PNP.

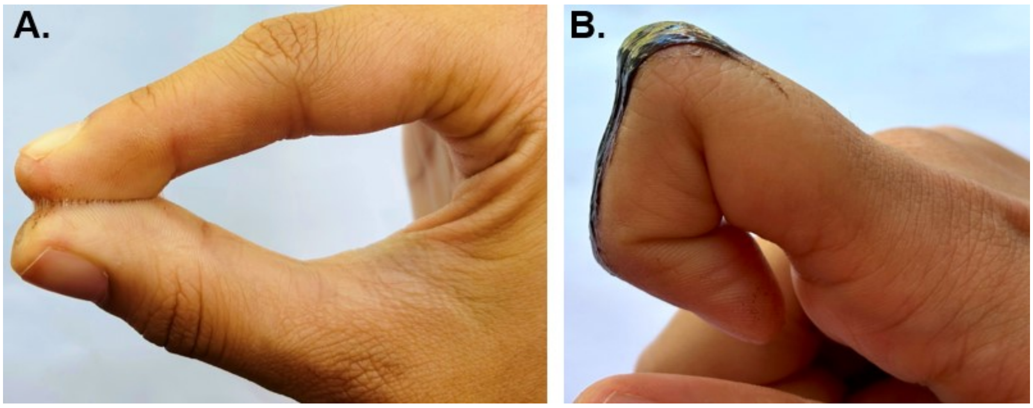

Fig. S9. Images with different concentrations of PNP sealant A. Acting as an appropriate sealant, and B. Potential to use as a patch.

Table S1. Comparison table of the recent strength of GelA reported from the lap shear test on porcine skin.

S. No.	**Formulations**	**Lap Sheer strength (MPa)**	**Reference cited in SI (Page S17-S18)**
1.	Proteinaceous Nanoparticle/TA (PNP sealant)	1.49	This work
2.	CD-CPD/TA adhesive	1.32	2
3.	Gelatin/polyacrylamide/CNT/TA	0.024	3
4.	GelMa/Polydopamine NP hydrogel	0.065	4
5.	GelMa–Gelatin/acetylcysteine electrospun fiber membrane	0.0016	5
6.	GelMA/Caffeic Acid	0.00015	6
7.	GelMA/platelet-rich fibrin/CD	0.150	7
8.	Gelatin/Acrylic acid/ hexadecenyl-1,2-catechol hydrogel (UV-initiated copolymerization)	0.063	8
9.	GelMA/poly (thioctic acid)/poly (acrylic acid)	0.255	9
10.	GelMA/Dopamine	0.001	10
11.	GelMA/methacrylate hyaluronic acid-Dopa Scaffold	0.011	11
12.	GelMA/ Zn^{2+}/chicken egg white	0.080	12
13.	Gelatin/thiolactone acrylamide/acrylic acid/GelMA	0.081	13
14.	Polyacrylamide/Gelatin/MXene	0.003	14
15.	Gelatin hydrogel/TA	0.036	15
16.	Gelatin/TA (underwater)	1.5	16
17.	PAM/Glycerol/Fe^{3+}/Gelatin/TA	0.098	17
18.	Gelatin/Hyaluronic Acid/TA	0.048	18
19.	PEG/Gelatin/TA	0.020	19

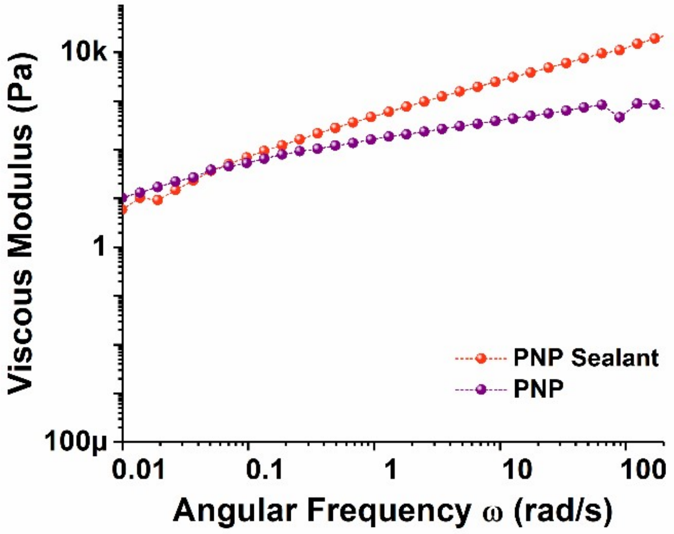

Fig. S10. PNP sealant has higher loss modulus.

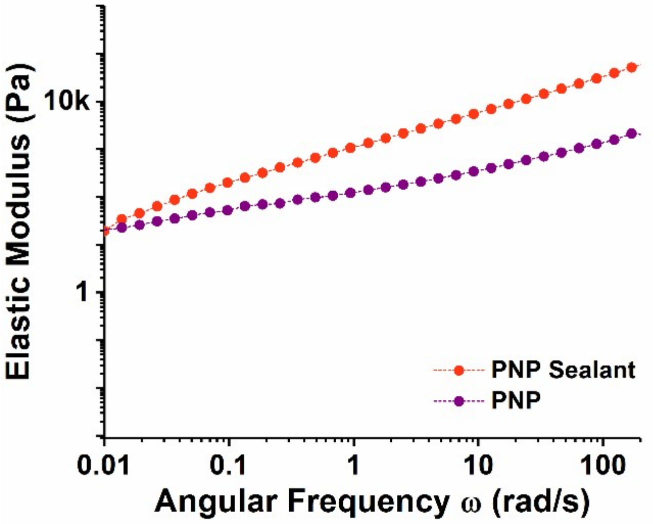

Fig. S11. Graph of storage modulus showing restricted mobility in PNP sealant compared to PNP.

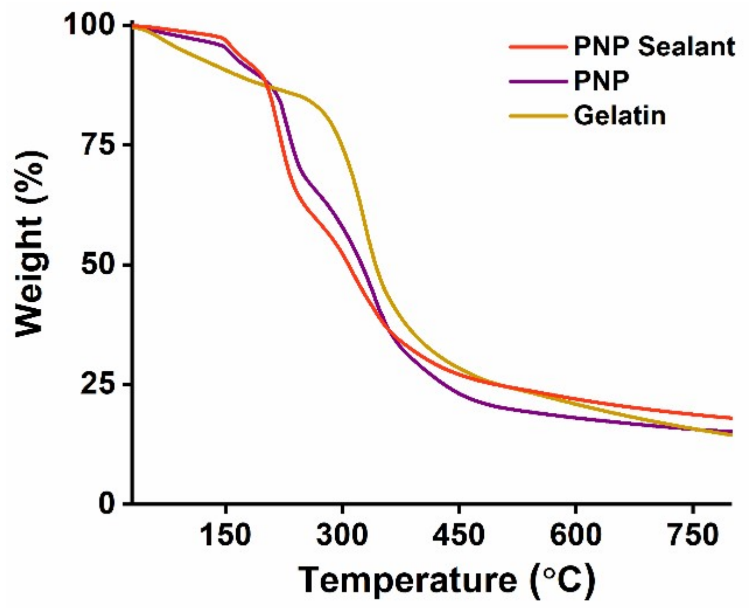

Fig. S12. TGA spectra displaying higher thermal stability of the PNP sealant.

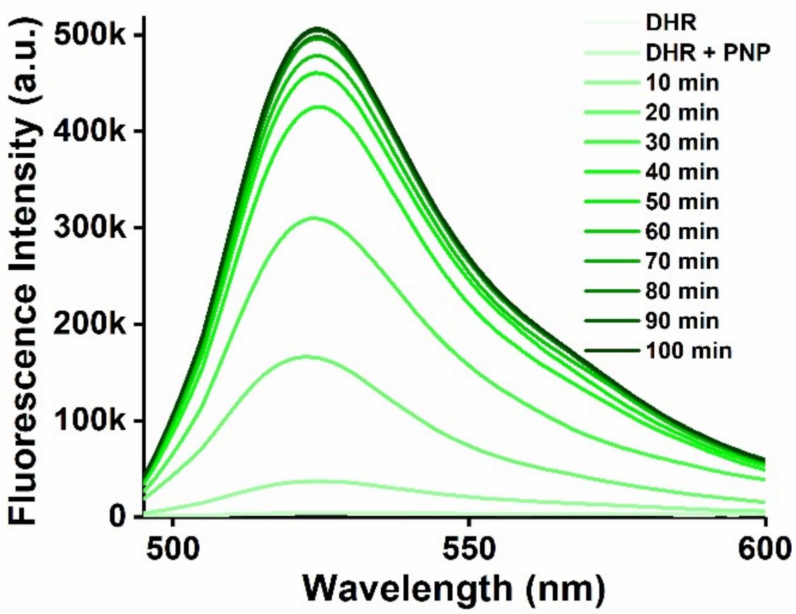

Fig. S13. Fluorescence spectra at 480 nm excitation of Rhodamine 123 converted from non-fluorescent DHR123 in the presence of pristine PNP under visible light irradiation, confirming ROS generation.

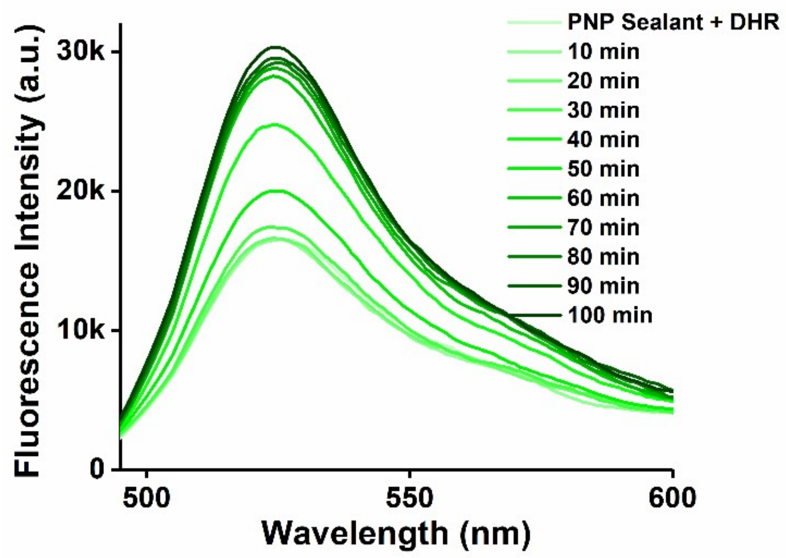

Fig. S14. Fluorescence spectra at 480 nm excitation of Rhodamine 123 converted from non-fluorescent DHR123 in the presence of PNP sealant under dark conditions, confirming suppressed ROS generation.

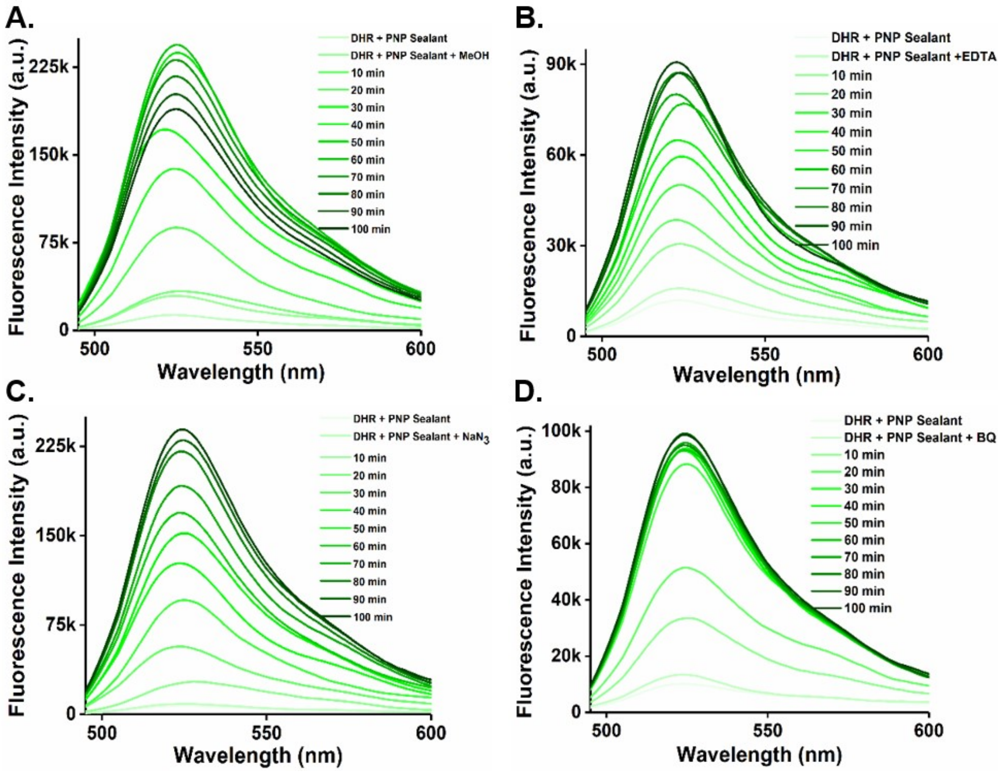

Fig. S15. PNP sealant A. Trapping of $^{\bullet}$OH using MeOH under visible light **B.** Trapping of surface-generated h^+ using Na_2-EDTA under visible light, C. Trapping of $^1O_2$ using NaN_3 under visible light, and D. Trapping of $^{\bullet}O^{2-}$ using BQ under visible light.

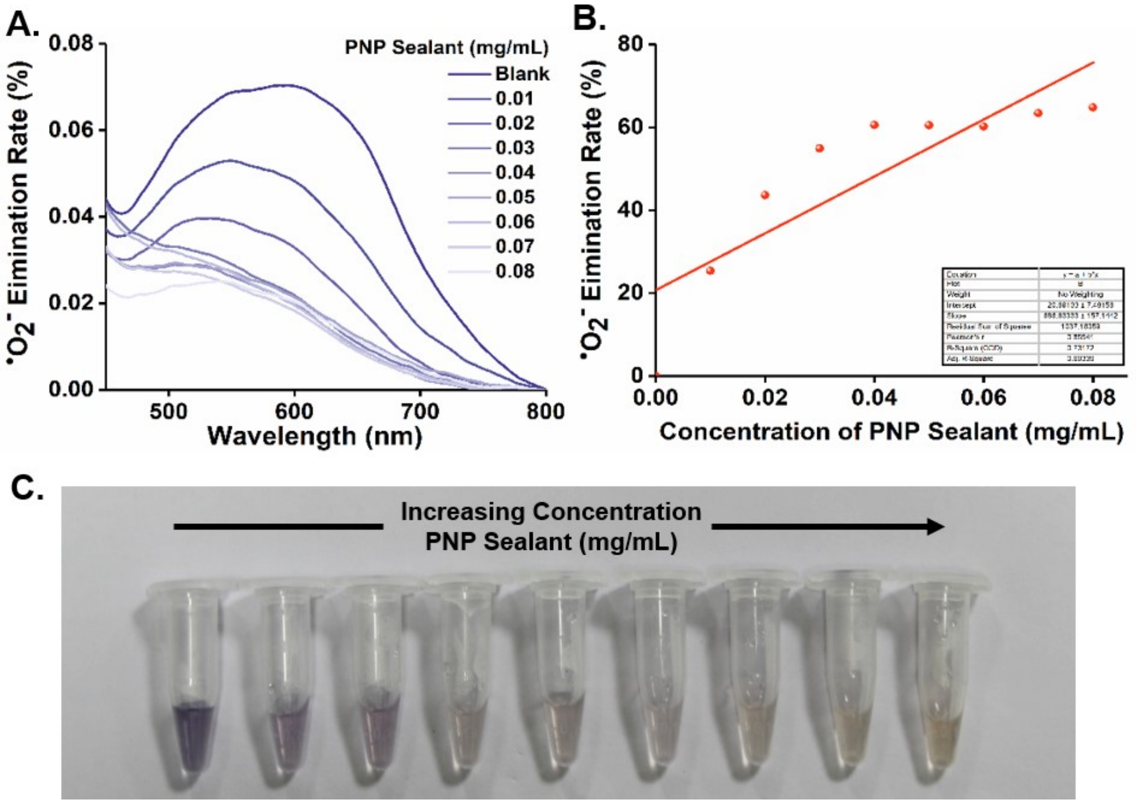

Fig. S16. NBT Assay of PNP sealant A. Concentration dependent UV-visible spectra, B. Linear fitting graph of IC_{50} value 0.042 mg/mL and C. Digital images of the assay.

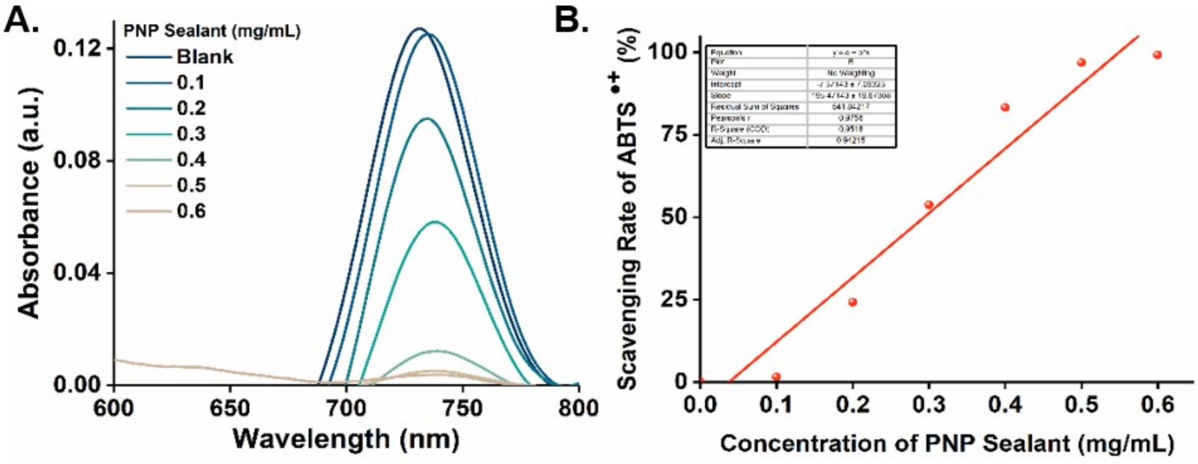

Fig. S17. PNP sealant ABTS assay A. Concentration dependent UV-visible spectra and B. Linear fitting graph IC_{50} value 0.293 mg/mL.

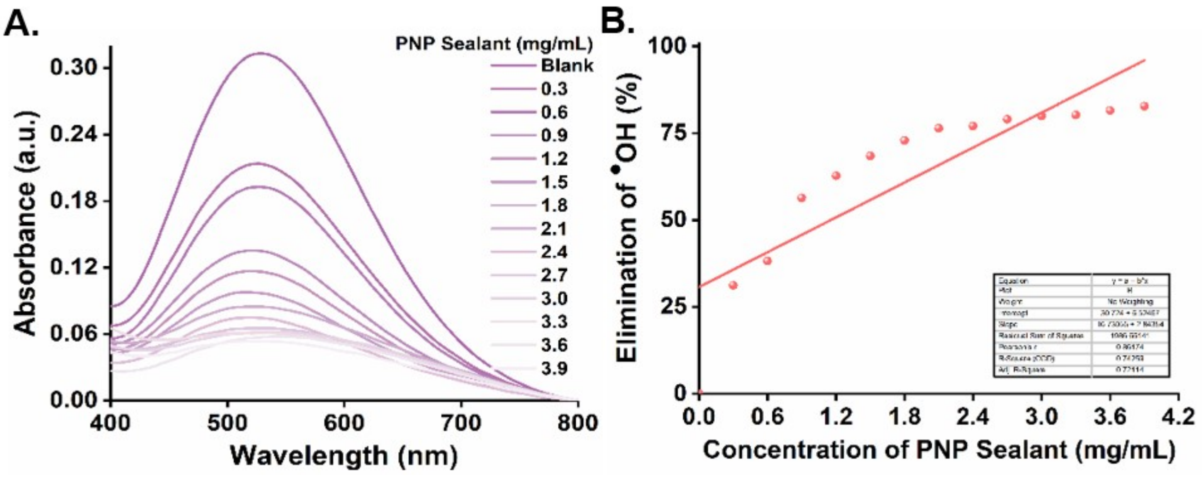

Fig. S18. PNP sealant A. UV-Visible spectra for •OH elimination study using Fenton reaction and B. EC_{50} of 1.15 mg/mL.

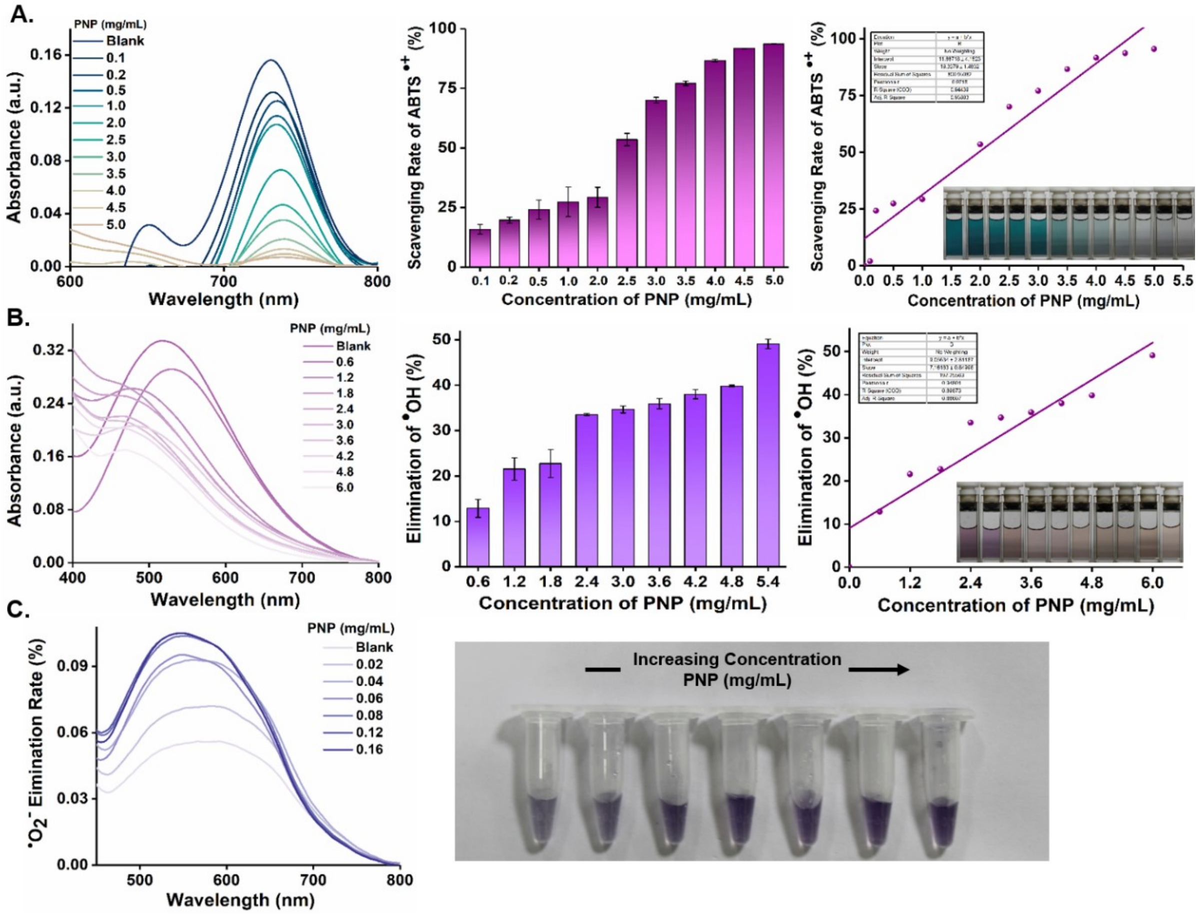

Fig. S19. Pristine PNP A. UV-Visible spectra for $ABTS^{+\bullet}$ assay, B. $ABTS^{+\bullet}$ maximum scavenging capacity of 95.54%, C. $IC_{50}$of 1.97 mg/mL, D. UV-Visible spectra for •OH activity, E.•OH maximum elimination efficacy 49.10%, F. Linear fitting graph of •OH activity, G. Showing no SOD activity, and H. Digital images of the SOD activity assay with increasing color.

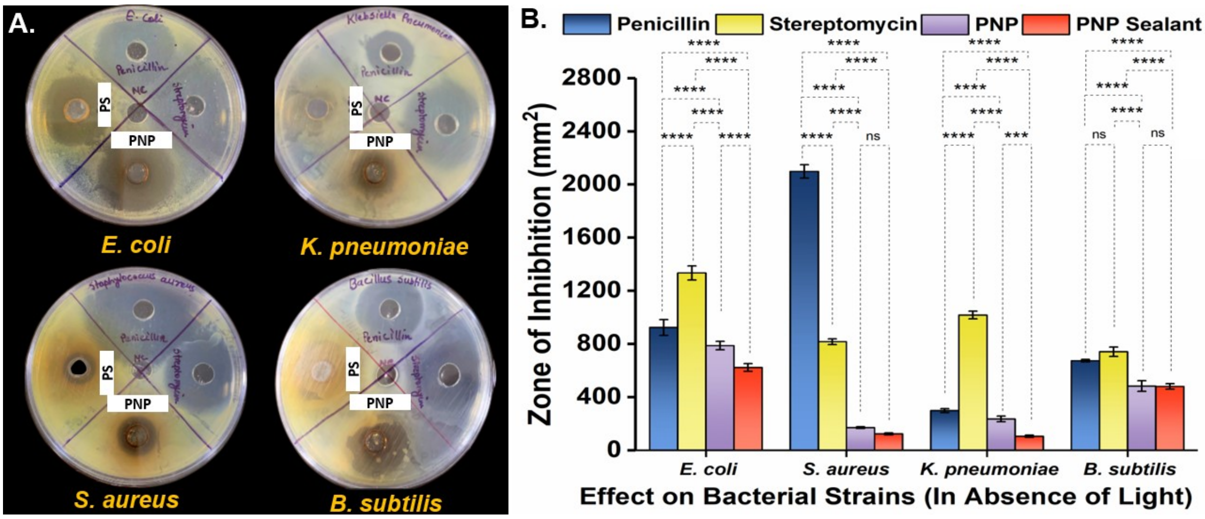

Fig. S20. Digital images of zone of inhibition studies on four bacterial strains under normal conditions (PCN: penicillin, SM: Streptomycin, PS: PNP sealant), and B. Area of zone of inhibition having high resistance towards *E. coli and B. subtilis*.

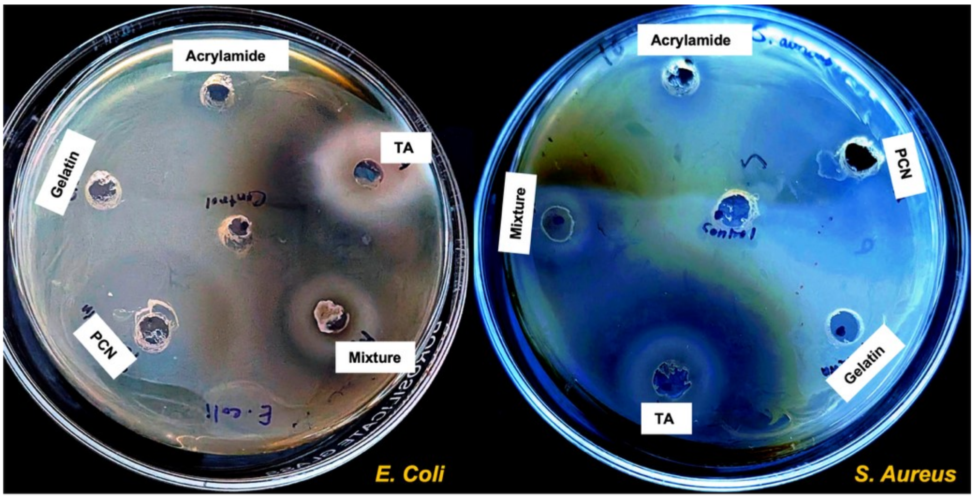

Fig. S21. Antibacterial activity tested against *E. coli* (Gram-negative) and *S. aureus* (Gram-positive) where TA and mixture of raw material shows weak activity while gelatin and acrylamide while gelatin and acrylamide doesn't show activity.

Table S2. Comparison table of antibacterial activity based on zone of inhibition area (mm^2) in light and dark conditions.

<table>
<tr><th colspan="5">In the presence of light</th></tr>
<tr><th></th><th>Penicillin</th><th>Streptomycin</th><th>PNP</th><th>PNP Sealant</th></tr>
<tr><td><i>E. coli</i></td><td>887.046 ± 5.28</td><td>990.2 ± 1.39E-13</td><td>871.293 ± 10.46</td><td>768.123 ± 2.83</td></tr>
<tr><td><i>S. aureus</i></td><td>1293.015 ± 3.67</td><td>1112.733 ±114.775</td><td>225.329± 6.17</td><td>116.983 ±5.04</td></tr>
<tr><td><i>K. pneumoniae</i></td><td>188.833 ± 8.49</td><td>996.353 ± 57.93</td><td>210.56 ± 10.64</td><td>68.616 ± 8.61</td></tr>
<tr><td><i>B. subtilis</i></td><td>492.41 ± 9.11</td><td>985.29 ± 63.26</td><td>513.883 ± 93.26</td><td>544.98 ± 20.79</td></tr>
<tr><th colspan="5">In the absence of light</th></tr>
<tr><td><i>E. coli</i></td><td>923.24 ± 59.56</td><td>1334.05 ± 53.17</td><td>786.46 ± 31.79</td><td>622.1 ± 28.78</td></tr>
<tr><td><i>S. aureus</i></td><td>2097.73 ± 50.75</td><td>816.44 ± 21.14</td><td>169.82 ± 6.14</td><td>122.85 ± 7.85</td></tr>
<tr><td><i>K. pneumoniae</i></td><td>297.86 ± 14.53</td><td>1016.53 ± 28.48</td><td>234.59 ± 21.82</td><td>104.62 ± 8.18</td></tr>
<tr><td><i>B. subtilis</i></td><td>673.02 ± 9.59</td><td>740.8 ± 34.94</td><td>482.5 ± 40.24</td><td>479.5 ± 20.43</td></tr>
</table>

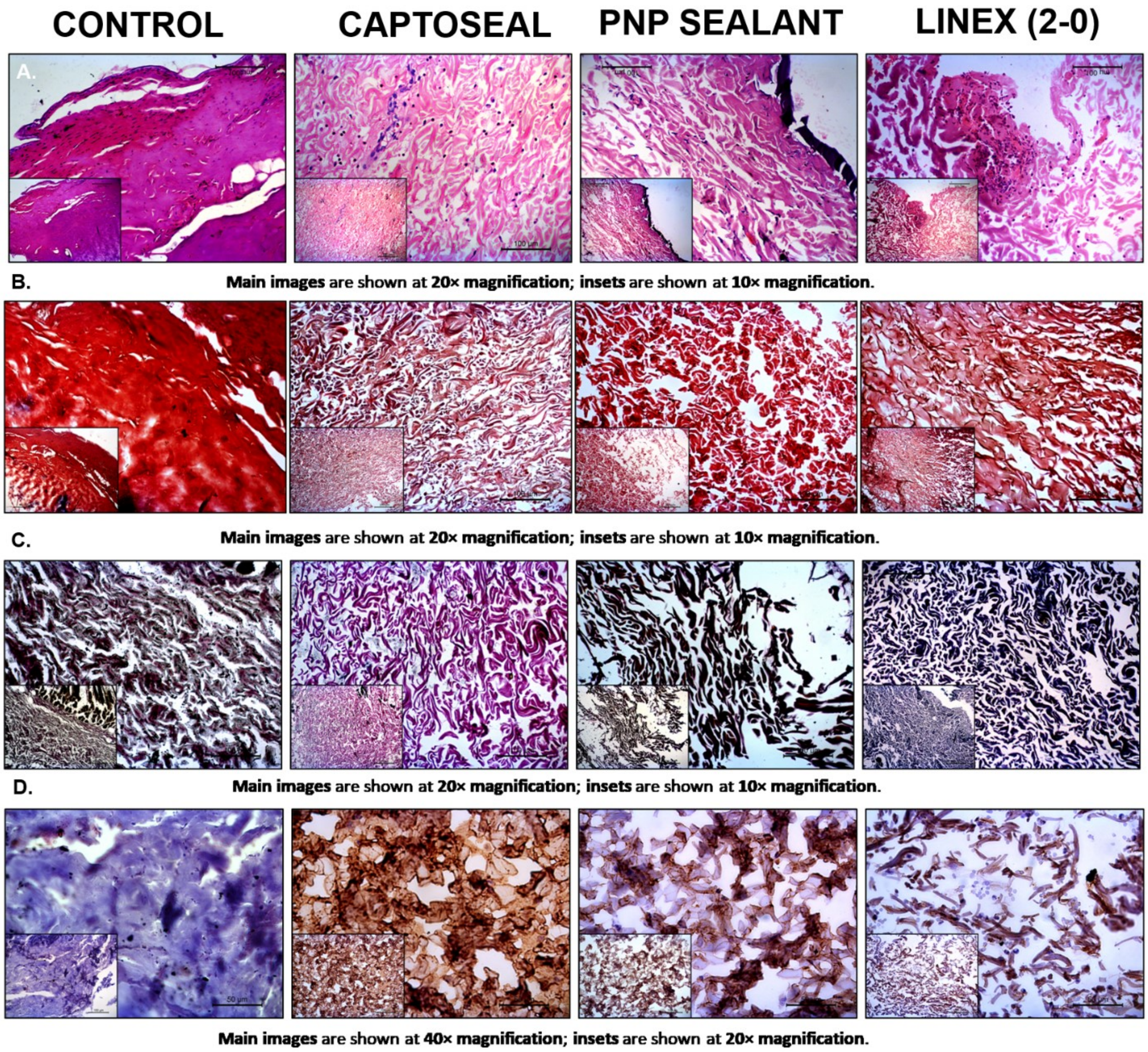

Fig. S22. Images of harvested healing skin samples at day 2: A. H&E staining, B. Masson trichrome staining, C. Reticulin fiber assessment, and D. Immunohistochemical staining against CD31.

References

1 D. Sridharan, N. Pracha, J. A. Dougherty, A. Akhtar, S. B. Alvi and M. Khan, *Methods Protoc.*, 2022, **5**, 13.

2 M. Aggarwal, D. Sharda, S. Srivastava, D. K. Kotnees, D. Choudhury and P. Das, *Small*, 2024, **20**, 2405531.

3 W. Liu, K. Wang, Z. Zhao, J. Yan, C. Zhang, S. Ma, J. Wang, W. Guo and J. Wang, *J. Mater. Chem. C*, 2024, **12**, 14330–14342.

4 S. Cheng, X. Zhang, J. Lu, K. Xiang, W. Zhang, W. Gao and M. Chen, *ACS Appl. Nano Mater.*, 2024, **7**, 17469–17481.

5 Y. Kong, H. Tang, H. Chai, L. Zhang, Z. Mao and H. Xu, *ACS Appl. Polym. Mater.*, 2025, **7**, 8383–8395.

6 H. Montazerian, S. Mitra, A. Hassani Najafabadi, R. Seyedmahmoud, Y. Zheng, M. R. Dokmeci, N. Annabi, A. Khademhosseini and P. S. Weiss, *ACS Mater. Lett.*, 2023, **5**, 1672–1683.

7 S. Ren, H. Lv, S. Chen, J. Zhou, S. Chen, J. Chen, J. Luo, Y. Guo, H. Wang, J. Zhai and Y. Zhou, *ACS Appl. Mater. Interfaces*, 2025, **17**, 20885–20900.

8 P. Ni, H. Huang, L. Zhang, Y. Chen, Z. Liang, Y. Weng, Y. Fang and H. Liu, *Adv. Healthc. Mater.*, 2023, **12**, 2203342.

9 M. Liang, D. Wei, P. Ren, L. Xu, Y. Tao, L. Yang, G. Jiao, T. Zhang and T. Serizawa, *Adv. Healthc. Mater.*, 2024, **13**, 2302538.

10 H. Montazerian, A. Baidya, R. Haghniaz, E. Davoodi, S. Ahadian, N. Annabi, A. Khademhosseini and P. S. Weiss, *ACS Appl. Mater. Interfaces*, 2021, **13**, 40290–40301.

11 S. Chen, M. L. Tomov, L. Ning, C. J. Gil, B. Hwang, H. Bauser-Heaton, H. Chen and V. Serpooshan, *Adv. Biol.*, 2023, **7**, 2300124.

12 Q. Li, Y. Hou, D. Sun, C. Zhu, R. Wu, G. Feng, L. Zhang and Y. Song, *ACS Appl. Mater. Interfaces*, 2025, **17**, 5719–5734.

13 J. Han, J. Park, R. Bhatta, Y. Liu, Y. Bo, J. Zhou and H. Wang, *Acta Biomater.*, 2022, **150**, 199–210.

14 J. Ma, H. Liang, W. Li, E. Liang and W. Zhang, *ACS Appl. Polym. Mater.*, 2025, **7**, 4549–4560.

15 Q. Zhao, S. Mu, Y. Long, J. Zhou, W. Chen, D. Astruc, C. Gaidau and H. Gu, *Macromol. Mater. Eng.*, 2019, **304**, 1–8.

16 Z. Yuan, T. Wang, C. Shao, S. Yang, W. Sun, Y. Chen, Z. Peng and Z. Tong, *Adv. Funct.*

Mater., 2025, **35**, 2412950.

17 X. Guo, W. Qin, C. Gu, X. Li, M. Chen, H. Zhai, X. Zhao, H. Liu, B. Zhao, Y. Zhang, Y. Wang and S. Yin, *Adv. Mater. Technol.*, 2024, **9**, 1–10.

18 H. Wang, M. Wang, J. Wu, S. Zhu, Y. Ye, Y. Liu, K. Li, R. Li, Y. Zhang, M. Wei, X. Yang and L. Meng, *Adv. Healthc. Mater.*, 2024, **2304444**, 1–14.

19 H. Li, Y. Shi, W. Zhang, M. Yu, X. Chen and M. Kong, *ACS Appl. Mater. Interfaces*, 2022, **14**, 18097–18109.